

Trapdoor viscous remanent magnetization

Karl Fabian¹

¹Norwegian University of Science and Technology (NTNU)

November 8, 2023

Abstract

Viscous remanent magnetization (VRM) in multidomain particles still exhibits many puzzling properties deviating from the current theory of VRM, based on Néel's single-domain model of magnetic particles with an almost symmetric double-well potential. In larger magnetic particles experimental evidence indicates that more complex magnetization structures preferentially change from high-energy states to low-energy states with large energy differences, such that VRM is preferentially acquired by directed magnetization changes in strongly asymmetric double-well potentials. Here a statistical model explains how this trapdoor VRM (tVRM) naturally explains the experimental observations of initial-state dependence, time-lag variation, non-linear log t dependence, and acquisition-decay asymmetry for multidomain VRM. It is discussed how tVRM can be experimentally distinguished from single-domain VRM and how the new theory can help to improve age determination by VRM analysis.

Trapdoor viscous remanent magnetization

Karl Fabian¹

¹Norwegian University of Science and Technology, Department of Geoscience, S. P. Andersens veg 15a,

Trondheim, Norway

ORCID: 0000-0002-3504-3292

Key Points:

- Multidomain viscous remanent magnetization (MD VRM) is dominated by decay into trapdoor potential minima
- Previously inexplicable properties of MD VRM are explained by a quantitative trapdoor VRM theory
- Trapdoor VRM suggests an improved methodology for VRM age determination

Corresponding author: Karl Fabian, karl.fabian@ntnu.no

Abstract

Viscous remanent magnetization (VRM) in multidomain particles still exhibits many puzzling properties deviating from the current theory of VRM, based on Néel's single-domain model of magnetic particles with an almost symmetric double-well potential. In larger magnetic particles experimental evidence indicates that more complex magnetization structures preferentially change from high-energy states to low-energy states with large energy differences, such that VRM is preferentially acquired by directed magnetization changes in strongly asymmetric double-well potentials. Here a statistical model explains how this trapdoor VRM (tVRM) naturally explains the experimental observations of initial-state dependence, time-lag variation, non-linear $\log t$ dependence, and acquisition-decay asymmetry for multidomain VRM. It is discussed how tVRM can be experimentally distinguished from single-domain VRM and how the new theory can help to improve age determination by VRM analysis.

Plain Language Summary

The magnetization of rocks is an important property used to determine the history of the Earth surface and the variation of the Earth magnetic field. It is mostly stored by small magnetite particles, which still are larger than about 500 nm in diameter and are called multidomain (MD) magnetites. If a rock, after its formation, lies at the Earth surface for a long time, its magnetization slowly changes and the remanent magnetization newly acquired is called viscous remanent magnetization (VRM). This VRM is very well understood for magnetite particles below about 150 nm in diameter, but no comprehensive theory so far explains all its experimentally observed properties. Here a statistical model is developed that can explain the experimental facts and helps to understand their physical origin. The new theory allows to theoretically investigate different methods to determine the amount of time a rock was exposed to the Earth magnetic field. This leads to a better understanding of time-temperature relations for VRM, and improves the determination of relocation ages based on VRM.

1 Introduction

Viscous remanent magnetization (VRM) is generated when a rock is exposed to a magnetic field for an extended time (Thellier, 1938). Single-domain (SD) VRM is explained by Néel theory (Néel, 1949b, 1949a), but for more complex magnetization struc-

43 tures, a comprehensive theory is missing (Dunlop, 1983; Tivey & Johnson, 1984; Moskowitz,
 44 1985; Williams & Muxworthy, 2006). Dunlop (1983) finds that room-temperature (RT)
 45 VRM is unexpectedly difficult to erase by heating, and that the viscosity coefficient S
 46 increases with time, which is now termed non- $\log(t)$ behavior (Halgedahl, 1993; Williams
 47 & Muxworthy, 2006). For natural rocks, Kent (1985) confirmed that SD blocking time-
 48 temperature relaxation theory (Pullaiah et al., 1975) underestimates thermal demagne-
 49 tization temperatures in Devonian limestones. Tivey and Johnson (1984) provided ex-
 50 tensive experimental data that VRM in MD samples is sensitive to the magnetic history
 51 of the samples, and that AF demagnetization decreases, while thermal demagnetization
 52 increases the ability of MD samples to acquire VRM. Also, both MD and SD samples
 53 are sensitive to zero and weak field storage duration Δt prior to the VRM measurement
 54 (Tivey & Johnson, 1984). These effects were confirmed for various samples in subsequent
 55 experimental studies (Moskowitz, 1985; Halgedahl, 1993; Muxworthy & Williams, 2006;
 56 Williams & Muxworthy, 2006; Yu & Tauxe, 2006).

57 Moskowitz (1985) distinguishes three main physical processes for these magnetic
 58 after-effects:

- 59 1. Thermal fluctuations (Dunlop, 1973) with diffusion constants S_a for VRM acqui-
 60 sition and S_d for decay.
- 61 2. Diffusion after-effect from relaxation due to vacancy/cation diffusion across en-
 62 ergy barriers (Street & Woolley, 1950; Kronmüller et al., 1974).
- 63 3. Disaccommodation, with a relaxation equation for magnetic susceptibility.

64 Moskowitz (1985) concludes that over geologic time, thermal fluctuations dominate VRM
 65 because the other two effects have relaxation times below 10 ka.

66 Central problems for MD VRM theory are the pronounced and universal non- $\log(t)$
 67 behavior, and the dependence of VRM acquisition on initial state and on waiting time
 68 Δt . Moon and Merrill (1986) studied these effects in terms of asymmetric potentials. Mi-
 69 croscopic studies of Halgedahl (1993) and Muxworthy and Williams (2006) found episodic
 70 random domain reorganization towards more stable magnetization states. The concept
 71 of trapdoor processes in VRM acquisition first occurs in relation to the long-term VRM
 72 observations by de Groot et al. (2014). VRM overshooting first occurred in a micromag-

73 netic study by Fabian and Shcherbakov (2018) and was explained by a statistical the-
 74 ory (Fabian, 2000, 2003).

75 Improving MD VRM theory is important for Holocene age determination, indepen-
 76 dent of radionuclides (Heller & Markert, 1973; Borradaile, 1996, 2003; Muxworthy et al.,
 77 2015; Berndt & Muxworthy, 2017; Sato et al., 2019). Recent VRM models mathemat-
 78 ically modify time-temperature relations to explain observed deviations from Néel the-
 79 ory Sato et al. (2016) suggest a mathematical modification of the time-temperature re-
 80 lation, or design concrete models of MD domain wall jumps Berndt and Chang (2018).

81 Here, a simplified theory quantifies MD VRM behavior including acquisition, de-
 82 cay, reorientation, and thermoviscous relations. It predicts an exponential decay that cu-
 83 mulatively depletes excited magnetization states of increasingly higher energy barriers,
 84 and helps to infer viscous magnetization ages using a new approach that is slightly dif-
 85 ferent from Néel theory.

86 2 Viscous magnetization in a double well potential

87 Micromagnetism describes physical magnetization structures as local energy min-
 88 ima (LEM). Viscous magnetization changes through thermal activation across an energy
 89 barrier between two LEM states S_1, S_2 . In Fig. 1a, energies E_1, E_2 , and magnetic mo-
 90 ments $\mathbf{m}_1, \mathbf{m}_2$ are denoted relative to energy $E = 0$ and moment \mathbf{m}_B at the energy bar-
 91 rier maximum.

92 If the probability of being in state S_i is ρ_i , then $\rho_1 + \rho_2 = 1$, and the kinetic equa-
 93 tion for the dynamic change of ρ_1 is

$$94 \quad \tau_0 \partial_t \rho_1 = -p_{12} \rho_1 + p_{21} \rho_2 = -(p_{12} + p_{21}) \rho_1 + p_{21}. \quad (1)$$

95 Here τ_0 is the attempt period (≈ 1 ns) and p_{ij} the probability to switch from S_i into S_j
 96 during τ_0 . For weak fields \mathbf{B} , not noticeably changing the magnetization at S_1, S_2 and
 97 the saddle-point, Arrhenius equation provides

$$p_{ij} = \exp - \frac{E_i + \mathbf{m}_i \mathbf{B}}{k T}.$$

98 Setting the left hand side of (1) to zero yields equilibrium state density and magnetiza-
 99 tion

$$\bar{\rho}_1 = \frac{p_{21}}{p_{12} + p_{21}}, \quad \bar{\mathbf{m}} = \mathbf{m}_1 \bar{\rho}_1 + \mathbf{m}_2 (1 - \bar{\rho}_1).$$

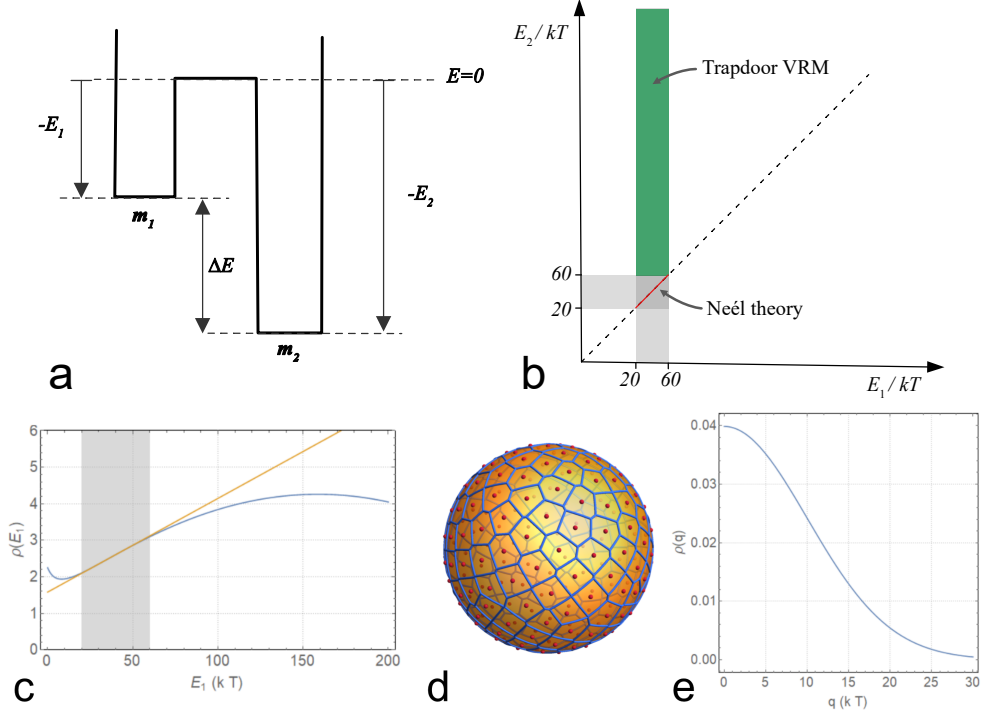


Figure 1. a) Energy barriers between two LEM states with barrier energies $E_1 \leq E_2$. In Neél-theory, the zero-field energies are equal, and the magnetic moments opposite, $E_1 = E_2$, $\mathbf{m}_1 = -\mathbf{m}_2$. For trapdoor-VRM theory it is assumed that $E_2 \gg E_1$ and no thermally activated transitions $2 \rightarrow 1$ occur. For an isotropic ensemble it then can be assumed that in the statistical average $\mathbf{m}_2 = 0$. b) Range of VRM zero-field energy barriers for Neél theory (red line) and trapdoor VRM (green). c) Approximation of a general energy barrier distribution $\psi_1(w)$ (blue) by a linear function (orange) in the small interval $[w_{\min}, w_{\max}] = [20, 60]$ (gray). d) Representation of the isotropic distribution of magnetic moment directions \mathbf{u} on the sphere by 200 nearly equi-distributed discrete directions (red) with their spherical Voronoi cells (blue). e) Gaussian distribution model of $\psi_3(q)$ for in-field energies $q > 0$ and $\sigma = 10$.

100 Solving the kinetic equation (1) for the disequilibrium density $\eta = \rho_1 - \bar{\rho}_1$, in time units
 101 of τ_0 yields

$$102 \quad \eta(t) = \eta_0 e^{-\lambda t}, \quad (2)$$

103 where

$$\lambda = p_{12} + p_{21} = \exp\left(-\frac{E_1 + \mathbf{m}_1 \mathbf{B}}{kT}\right) + \exp\left(-\frac{E_2 + \mathbf{m}_2 \mathbf{B}}{kT}\right)$$

104 is the constant of exponential decay towards $\bar{\rho}_1$. Note, that substituting λ into (2) leads
 105 to two nested exponentials which are the primary source of complications when analyz-
 106 ing VRM.

107 In Néel's theory of SD VRM (sVRM) the micromagnetic energy landscape has only
 108 two minima of equal energy $E_1 = E_2$ and opposite magnetic moments $\mathbf{m}_2 = -\mathbf{m}_1$.
 109 In contrast, trapdoor VRM (tVRM) assumes that E_1 and E_2 are very different, and math-
 110 ematically corresponds to the limit $E_2 \rightarrow \infty$ where

$$\bar{\rho}_1 \rightarrow 0, \quad \lambda \rightarrow \exp\left(-\frac{E_1 + \mathbf{m}_1 \mathbf{B}}{kT}\right).$$

111 By introducing the scaled zero-field barrier $w = E_1/(kT)$, the field energy amplitude
 112 $q = mB/(kT)$, and the angular component $\mathbf{u} \cdot \mathbf{b} = \cos\theta$ of the magnetic moment
 113 $\mathbf{m}_1 = m\mathbf{u}$ and the field $\mathbf{B} = B\mathbf{b}$, with unit vectors \mathbf{b} and \mathbf{u} , the decay constant be-
 114 comes

$$\lambda = \exp\left(-(w + q\mathbf{u} \cdot \mathbf{b})\right). \quad (3)$$

115 **3 Theory of trapdoor VRM**

116 The key observation in Néel's theory of SD TRM is that the small range 20-60 of
 117 energy barriers E/kT contains all relevant blocking times from the laboratory time scales
 118 of about 1 s to geological time-scales of 4 Ga. At RT, only these barriers contribute to
 119 VRM acquisition (Fig. 1b).

120 Only in SD or small pseudo-single domain (PSD) particles do such low barrier en-
 121 ergies systematically occur between LEMs with $E_1 \approx E_2$ (red line in Fig. 1b). In larger
 122 PSD and MD particles, it is far more likely that for the deeper LEM one has $E_2 \gg 60 kT$
 123 (green area in Fig. 1b), and with overwhelming probability, thermally activated processes
 124 only lead from the high-energy state E_1 to the low-energy state E_2 . This phenomenon
 125 has been compared to a trapdoor in de Groot et al. (2014). A specific example for a trap-
 126 door VRM process is the flower-vortex (F111-V100) transition studied and explained in

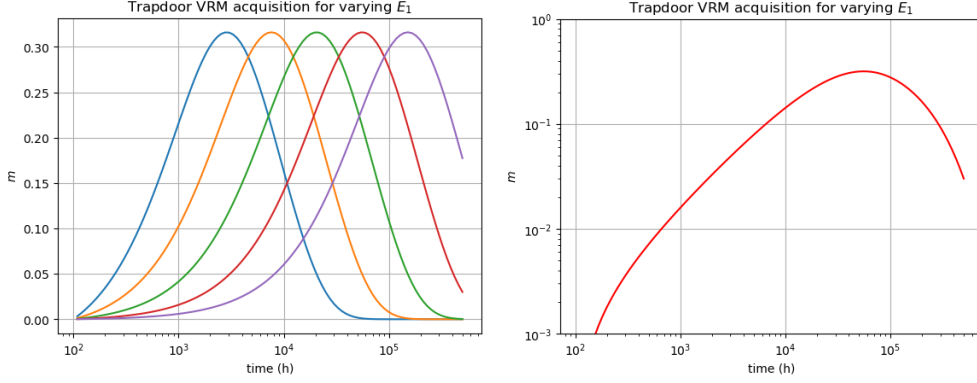


Figure 2. Left: Modeled tVRM acquisition by two oppositely magnetized states $\mathbf{u} \cdot \mathbf{b} = \pm 1$ with $q = 1 kT$ for different values of $E_1 \in [37, 38, 39, 40, 41] kT$ (blue to violet curves). Right: The log-log plot of the left red curve for $E_1 = 40 kT$ shows nearly linear increase up to about 2×10^4 h (2.3 a) due to the initial depletion of the misaligned states. Only after about 200 a also the aligned states largely are depleted.

127 Fabian and Shcherbakov (2018) based on micromagnetically calculated energy barriers
 128 of a PSD magnetite cube.

129 While sVRM results from an equilibrium within the current field, tVRM describes
 130 an irreversible depletion of high-energy LEMs, where opposite magnetizations with equal
 131 zero-field energy decay over different time scales in field. Intermediate tVRM is acquired
 132 because field-aligned states become slightly more stable, and their equally probable in-
 133 verse states decay faster. But once the field-aligned states decayed away, the final tVRM
 134 for one value of E_1 is zero. However, new intermediate tVRMs for higher energy bar-
 135 riers are synchronously acquired, such that the measured VRM over time is dynami-
 136 cally carried by different magnetic moments belonging to increasing energy barriers. Whether
 137 this on average increases the measured VRM depends on the sample-specific state-probability
 138 distribution and on the initial occupancy of the different LEMs. That an increase in VRM
 139 with time is most common is probably due to very long half-lives of misaligned moments
 140 for VRM processes with large q .

141 For example, assume two oppositely magnetized states with $E_1 = 40 kT$, $q =$
 142 $1 kT$, and $\mathbf{u} \cdot \mathbf{b} = \pm 1$. The red curve in Figure 2 displays the VRM acquired and lost
 143 by this configuration over time. In the beginning, the states acquire VRM according to
 144 a $\log t$ law because the state inverse to the external field with barrier $w - q = 39$ de-

145 cays first. After 6-7 a the field-aligned states with $w+q = 41$ also decay away and the
 146 VRM decreases until after about 100 a it has almost completely vanished. The math-
 147 ematical similarity of tVRM and radionuclide decay suggests that tVRM also may be
 148 useful for age determination.

149 **4 Modeling trapdoor VRM**

150 For quantifying tVRM it is assumed that in the parameter range of interest w , q
 151 and \mathbf{u} are statistically independent. The sample specific state-probability density then
 152 factors into

$$\psi(w, \mathbf{u}, q) = \psi_1(w) \psi_2(\mathbf{u}) \psi_3(q).$$

153 Figure 1c illustrates that the density of zero-field barriers $w = E_1/kT$ on the small in-
 154 terval $[w_{\min}, w_{\max}] = [20, 60]$, can be approximated by a linear state density

$$\psi_1(w) = \frac{1}{w_{\max} - w_{\min}} + \alpha \left(w - \frac{w_{\max} + w_{\min}}{2} \right).$$

155 For an isotropic sample, $\psi_2(\mathbf{u})$ is constant on the unit sphere. This is numerically mod-
 156 eled by a sufficiently large number of nearly equi-distributed discrete directions on the
 157 sphere, each weighted by the area of its Voronoi cell (Fig. 1d). Because the state den-
 158 sity $\psi_3(q)$ of the external-field energy q should decay away quickly for large q , it is here
 159 modeled by the positive normal distribution

$$\psi_3(q) = \frac{2}{\sqrt{2\pi} \sigma} e^{-\frac{q^2}{2\sigma^2}},$$

160 with width σ (Fig. 1e).

161 The function $\psi(w, \mathbf{u}, q)$ provides the probability for the occurrence of a LEM with
 162 parameters w , \mathbf{u} , q in the sample, but not the statistical occupancy of these states, which
 163 depends on the magnetic history of the sample. Starting from an initial state occupancy
 164 $\rho_0(w, \mathbf{u}, q)$, its evolution is described by

$$\rho(w, \mathbf{u}, q, t) = \rho_0(w, \mathbf{u}, q) \psi(w, \mathbf{u}, q) \exp\left(-t e^{-(w+q(\mathbf{u}\cdot\mathbf{b}))}\right). \quad (4)$$

165 The numerical models below assume an initially constant state occupancy ρ_0 on the rel-
 166 evant tVRM parameter interval, which approximately represents a thermally demagne-
 167 tized or a weak field TRM state, assuming that the TRM reflects only a small deviation
 168 from the equilibrium absolute zero state. AF demagnetized or ARM states may have dif-
 169 ferent initial state occupancies, where low energy barriers w and larger q states are less

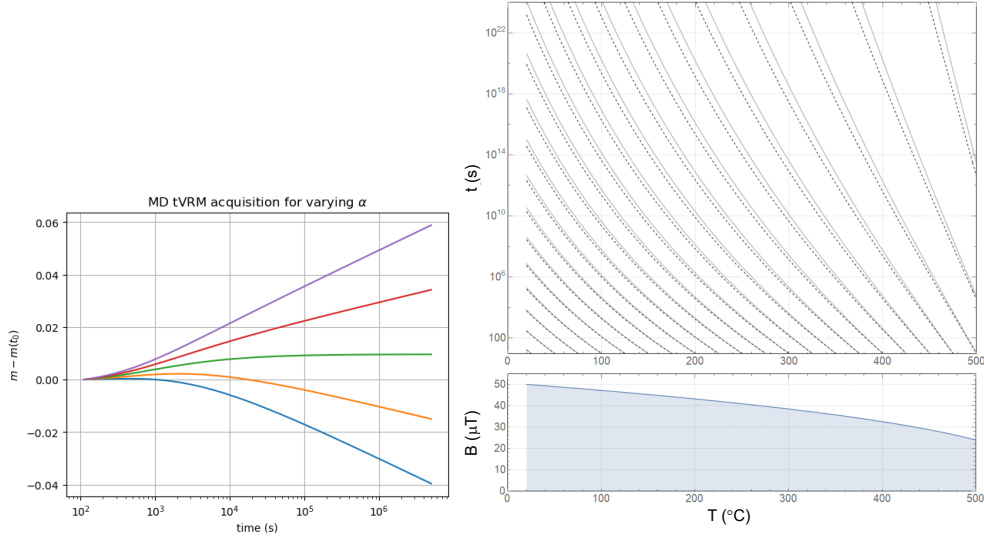


Figure 3. Left: Modeled tVRM acquisition for different values of α in the state-probability $\psi_1(w)$. The shown model uses the parameters $\sigma = 5$, $w \in [20, 80]$ and $\alpha = [-1, -0.5, 0, 0.5, 1]/(w_{max} - w_{min})^2$ for the plots from blue to violet. The model run starts after an initial 500 s VRM acquisition. Note that a decreasing state-probability with increasing w (blue, orange) can lead to decreasing VRM in a positive field, due to the fact that depletion of the field mis-aligned low- w states is not dynamically balanced by larger VRM acquisition of high- w barriers. Right top: Time-temperature diagram for tVRM decay times in MD magnetite calculated using equation (6) for two different critical exponents γ of $M_s(T)$: $\gamma = 0.38$ (solid gray), $\gamma = 0.36$ (dashed). Right bottom: Required change of applied field as a function of temperature to retain correct tVRM scaling for initial field $B_0 = 50 \mu\text{T}$ at RT.

170 populated than larger w and lower q states. In very old rocks, the 'trapdoor'-components
 171 of VRM are already largely activated and trapped in their low-energy minima, such that
 172 ρ_0 will be extremely reduced for smaller w .

173 5 Recovering the tVRM activation history

174 Because tVRM is a combination of many simple decay processes, to recover the VRM
 175 history of a rock, it appears promising to measure which energy levels of LEMs have al-
 176 ready been depleted during the time of the rock emplacement. The simplest procedure
 177 to measure this would be to again acquire VRM in the same external field for an extended
 178 period of time and then identify at what point an increase in VRM acquisition is detected.
 179 At this time, new LEM barriers that have not been depleted previously are activated.

180 Curves like those in Fig. 4 (top right) can then be used to calibrate the experimental data,
 181 and infer a viscous-remanence age from the rock.

182 Unfortunately, VRM of interesting processes was acquired on historical and geo-
 183 logical time scales, such that this direct approach is not practical and needs to be replaced
 184 by an alternative way to activate higher energy barriers. The classical procedure in Néel
 185 theory is to increase the measurement temperature and use time-temperature relations
 186 (Pullaiah et al., 1975; Heller & Markert, 1973) to convert between these quantities.

187 For tVRM acquired by MD magnetite well below the Curie temperature $T_C \approx 580^\circ\text{C}$
 188 the zero-field micromagnetic energy is dominated by the demagnetizing energy which scales
 189 with $K_d(T) = \frac{1}{2} \mu_0 M_s(T)^2$, such that

$$\frac{E_1(T)}{K_d(T)} = w \frac{kT}{K_d(T)}$$

190 is almost independent of T . Using the saturation magnetization $M_{s,0}$ at 0 K, and the
 191 critical exponent $\gamma \approx 0.37$ one has

$$M_s(T) = M_{s,0} (1 - T/T_C)^\gamma,$$

192 and with

$$\beta(T) = \frac{kT}{K_d(T)} \frac{K_d(T_0)}{kT_0} = \frac{T}{T_0} \left(\frac{T_C - T_0}{T_C - T} \right)^{2\gamma},$$

193 one can write $w(T) \approx w\beta(T)$. In experiments the same scaling behavior for $q = mB$
 194 is achieved by decreasing the applied field strength according to

$$195 \quad B(T) = B(T_0) \frac{M_s(T)}{M_s(T_0)}. \quad (5)$$

196 The temperature dependence of the decay constant in (3) is then

$$\lambda(T) = \lambda^{\beta(T)}.$$

197 If at temperature T , the laboratory decay time $t_L = 1/\lambda(T)$ activates the same
 198 energy barriers as a RT decay time of $t = 1/\lambda(T_0)$ one gets

$$\frac{\log t/\tau_0}{\log t_L/\tau_0} \approx \frac{1}{\beta(T)}.$$

199 For $t_L = 10$ s one has $\log t_L/\tau_0 = 23$ with the time-temperature relation

$$\log t/\tau_0 \approx 23 \frac{T M_s^2(T_0)}{T_0 M_s^2(T)}. \quad (6)$$

200 This agrees with the time-temperature relation derived from Néel theory for pure shape
 201 anisotropy (Pullaiah et al., 1975), because also in this case only demagnetizing energies
 202 are considered. Yet, equation (6) applies to different magnetization processes where the
 203 laboratory field is aligned with the natural VRM overprinting field and changes accord-
 204 ing to the scaling (5). The cumulative depletion of high-energy LEMs generates a sub-
 205 stantially different magnetization behavior than the predictions based on Néel theory,
 206 although also in the sVRM case for magnetite, VRM at elevated temperatures should
 207 be acquired in the correctly scaled field $B(T)$.

208 Fig. 3(right) demonstrates that this relation predicts a sensitive dependence of tVRM
 209 acquisition on temperature and heating rate. Using thermal tVRM acquisition as a dat-
 210 ing tool therefore requires very careful experiments allowing for accurate control of the
 211 measurement conditions in terms of temperature, measurement time, and thermal equi-
 212 libration.

213 In the supplementary material the Python code for a numerical model is provided
 214 that allows to simulate arbitrary time-temperature and field histories for magnetite MD
 215 ensembles based on the assumption of initially nearly constant probability density.

216 If the magnetization of a rock was displaced from an initial orientation \mathbf{m}_A to a
 217 new orientation \mathbf{m}_B it starts to realign its VRM with the current field H .

218 6 Discussion

219 The tVRM model describes a depletion of LEM states with elevated energy by means
 220 of a decay equation, and appears simpler than Néel's sVRM theory. What complicates
 221 the tVRM model, is the statistical decoupling of magnetic moment vectors and energy
 222 barriers. The corresponding evolution of $\rho(w, \mathbf{u}, q, t)$ naturally explains the experimen-
 223 tally observed deviations of MD VRM from Néel theory. The modeling of tVRM is com-
 224 plex, because the integration over the decay equations for all energy barriers and mag-
 225 netic moments cannot be done analytically and requires numerical treatment. The most
 226 notable property of tVRM is that it statistically approaches zero as depicted in Fig. 2,
 227 whilst sVRM attains a non-zero equilibrium. The visible tVRM is carried by changing
 228 magnetic moments from successively increasing energy barriers. Accordingly, the VRM
 229 magnetization curves depend on the distribution and initial occupation of these energy
 230 barriers. In Fig. 3(left) the dependence of the slope of the tVRM acquisition curves on

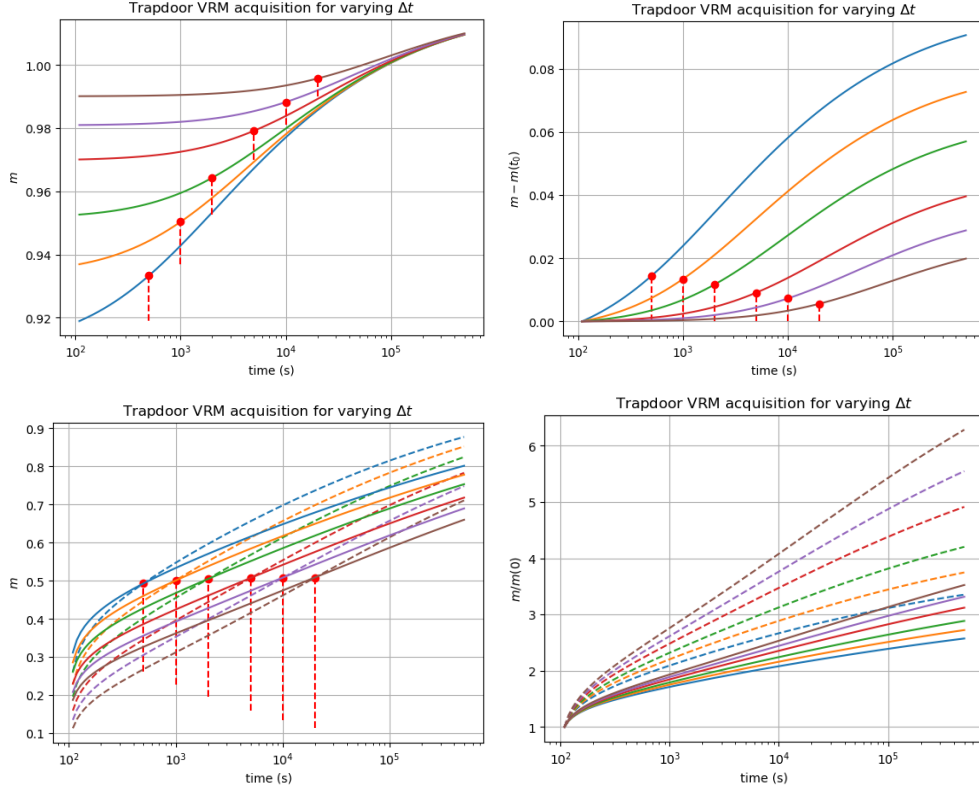


Figure 4. Top left: Modeled tVRM acquisition in an MD sample with initial density defined by $\alpha = 0$, $\sigma = 10$ and VRM acquisition in x-direction for $\Delta t = 0.5, 1, 2, 5, 10, 20 \times 10^3$ s (sequence blue to brown). The plot shows the results of a repeated VRM acquisition in x-direction after this history. Note the marked non- $\log(t)$ behavior and the systematic dependence on the previous Δt marked by red dots. Top right: The same data after subtracting the initial magnetization to simplify comparison to experiments. Bottom Left: Same as top left, but with initial density after VRM in zero field (dashed lines) or in perpendicular y -direction (solid lines) for $\Delta t = 0.5, 1, 2, 5, 10, 20 \times 10^3$ s (sequence blue to brown). Bottom right: The same data as on the left after subtracting the initial magnetization.

231 the slope α of the zero-field energy distribution $\psi_1(w)$ is plotted. The results demonstrate
 232 that tVRM acquired in a positive field may even decrease with time. To what extent de-
 233 tails of the distributions ψ_1 and ψ_3 systematically depend on grain size, shape or other
 234 average quantities of the magnetic particle ensemble is unclear and requires further study,
 235 preferably by micromagnetic models (Conbhuí et al., 2018; Fabian & Shcherbakov, 2018).

236 A significant deviation from Néel theory is that MD VRM acquisition strongly de-
 237 pends on initial state. sVRM usually starts from a near equilibrium of two equal zero-
 238 field energy states, and evolves towards an only slightly different equilibrium. In con-
 239 trast, tVRM is a pure depletion process modified by the external field. Figure 4 displays
 240 model runs which demonstrate that tVRM acquisition depends strongly on the initial
 241 population of the high-energy LEMs. The top row shows tVRM acquisition curves af-
 242 ter a previous tVRM acquisition in the same direction, that partly depleted the low- w
 243 states with field-aligned magnetic moments. tVRM during a second acquisition in the
 244 same direction depends on the degree of the first depletion and leads to s-shaped acqui-
 245 sition curves, resembling various experimental results, for example in figures 4,6,7 of (Moskowitz,
 246 1985), figure 2 in (Bikova & Igoshin, 1985), and figures 1,8 in (Lowrie & Kent, 1978).

247 High activation energy during AF demagnetization of MD samples leads to a lower
 248 occupation probability of low- w LEMs than thermal demagnetization. This explains why
 249 AF or ARM states in MD samples acquire less VRM than thermally demagnetized or
 250 TRM states.

251 The tVRM model calculations can show both, marked non- $\log t$ behavior and straight
 252 $\log t$ behavior, at least over extended time intervals. Non- $\log t$ behavior typically results
 253 from partly depleted initial states, where over long time-scales larger energy barriers are
 254 activated, that block LEMs with higher occupation probability. Another source of non-
 255 $\log t$ behavior can be strongly varying energy barrier distributions in the active region.
 256 For tVRM the physical origin of the magnetic energy barrier is irrelevant for the statisti-
 257 cal behavior of the sample, such that also diffusion after-effects from vacancy or cation
 258 diffusion (Street & Woolley, 1950; Kronmüller et al., 1974) and disaccommodation pro-
 259 cesses (Moskowitz, 1985) are described by the tVRM model. On some time scales these
 260 effects may substantially increase the energy barrier density.

261 The waiting time Δt effect in principle occurs even for the simple $\log t$ -law

$$M(t) - M_0 = S \log t, \text{ for } t > t_0,$$

262 because it predicts a VRM

$$M_{\Delta t}(t) = M(t + \Delta t) - M(\Delta t) \approx M(t) - S \log(\Delta t),$$

263 that shows a 'hardening effect' (Dunlop, 1983) due to the asymptotic downward shift $S \log \Delta t$.

264 The tVRM model predicts a a strong Δt effect due to the irreversible depletion of LEMs
 265 in contrast to the reversible equilibrium shift in the sVRM model. This is leads to a sys-
 266 tematic variation in Fig. 4 which contains plots of modeled tVRM acquisitions after dif-
 267 ferent previous acquisition periods Δt .

268 **6.1 Combinations of sVRM and tVRM**

269 In samples with different magnetic grain size populations, both types, sVRM and
 270 tVRM, may be present in various combinations. Especially for age determination, it is
 271 of interest to separate these two components into

$$VRM = sVRM + tVRM.$$

272 To design methods to identify the more reversible behavior of sVRM is the aim of fu-
 273 ture experimental studies. The region in Fig. 1b off the red diagonal, where both asym-
 274 metric barriers are below $60 kT$ may require separate treatment in certain narrow PSD
 275 particle ensembles. This requires the more comprehensive but also more complex Markov
 276 chain methods (Fabian & Shcherbakov, 2018). The simpler theory of tVRM focuses on
 277 MD particle ensembles, and on ensembles with large grain size variation.

278 The observation that isothermal VRM is overly difficult to erase by heating (Dunlop,
 279 1983; Kent, 1985) finds a natural explanation in tVRM, where a magnetic moment is al-
 280 most impossible to move back from a trapped state. To erase such a tVRM with bar-
 281 rier $w-q$ it is necessary that the field-aligned magnetizations with their larger in-field
 282 barrier $w+q$ or zero-field barrier w also decay into their trapped states, which requires
 283 higher temperatures than expected for a $w - q$ barrier.

284 Because tVRM results from a dynamic decay that depletes the occupation prob-
 285 abilities for successively larger energy barriers w , those low- w LEMs that have been de-
 286 pleted cannot be easily occupied again. It is therefore possible to experimentally deter-
 287 mine the degree of depletion, and from that infer the time it took to reach this state of
 288 depletion. To do this one has to find a measurable difference between depleted and oc-
 289 cupated LEMs, which naively can be done by simply repeating the VRM acquisition in

290 the same external field, and wait until an accelerated tVRM acquisition is observed. Of
 291 course, waiting times of thousands of years are unpractical, and thus the time-temperature
 292 relation (6) can be used to replace waiting time through measurements at elevated tem-
 293 peratures. To keep the correct scaling, the applied field strength in these measurements
 294 must be scaled down, according to (5). Calibration curves for such dating methods, could
 295 be developed based on the here presented programs and additional rock magnetic mea-
 296 surements that constrain the LEM state-distribution function ψ .

297 If tVRM prevails in a rock sample, its VRM acquisition depends strongly on the
 298 initial occupation and state-densities ρ_0, ψ , and there exists little reliable data to real-
 299 istically constrain these functions. Thus, the tVRM concept provides a new incentive and
 300 guideline to design targeted experimental and micromagnetic studies to determine re-
 301 alistic density distributions ψ_1 and ψ_3 . This will enable a better understanding of VRM
 302 processes, improve existing and help to develop new methods of age determination, ei-
 303 ther directly based on tVRM, or by better isolating the contribution of sVRM.

304 7 Open Research

305 The Python code used to model the VRM processes is available in the supporting
 306 information. If requested, the code will eventually be deposited at the NTNU repository
 307 (dataverse.no) by the time the article is accepted.

308 Acknowledgments

309 References

- 310 Berndt, T., & Chang, L. (2018). Theory of stable multi-domain thermoviscous rema-
 311 nence based on repeated domain-wall jumps. *Journal of Geophysical Research:*
 312 *Solid Earth*. doi: 10.1029/2018jb016816
- 313 Berndt, T., & Muxworthy, A. R. (2017). Dating Icelandic glacial floods using a new
 314 viscous remanent magnetization protocol. *Geology*, *45*(4), 339–342. doi: 10
 315 .1130/g38600.1
- 316 Bikova, E., & Igoshin, L. (1985). On the interrelation between magnetic viscos-
 317 ity and the compositions of magnetites in the alkali-ultrabasic rocks the Kola
 318 peninsula. *Izvestiya. Earth Phys.*, *21*, 794-800.

- 319 Borradaile, G. J. (1996). An 1800-year archeological experiment in remagnetization.
320 *Geophysical Research Letters*, *23*(13), 1585–1588. doi: 10.1029/96gl01575
- 321 Borradaile, G. J. (2003). Viscous magnetization, archaeology and Bayesian statis-
322 tics of small samples from Israel and England. *Geophysical Research Letters*,
323 *30*(10), 4. doi: 10.1029/2003gl016977
- 324 Conbhuí, P. Ó., Williams, W., Fabian, K., Ridley, P., Nagy, L., & Muxworthy,
325 A. R. (2018). MERRILL: Micromagnetic earth related robust interpreted
326 language laboratory. *Geochemistry, Geophysics, Geosystems*, *19*. doi:
327 10.1002/2017gc007279
- 328 de Groot, L. V., Fabian, K., Bakelaar, I. A., & Dekkers, M. J. (2014). Magnetic
329 force microscopy reveals meta-stable magnetic domain states that prevent
330 reliable absolute palaeointensity experiments. *Nature Communications*, *5*.
- 331 Dunlop, D. J. (1973). Theory of the magnetic viscosity of lunar and terrestrial rocks.
332 *Reviews of Geophysics*, *11*(4), 855. doi: 10.1029/rg011i004p00855
- 333 Dunlop, D. J. (1983). Viscous magnetization of 0.04–100 μm magnetites. *Geophys.*
334 *J. R. astr. Soc.*, *74*(4), 667–687.
- 335 Fabian, K. (2000). Acquisition of thermoremanent magnetization in weak magnetic
336 fields. *Geophysical Journal International*, *142*(2), 478–486.
- 337 Fabian, K. (2003). Statistical theory of weak field thermoremanent magnetization
338 in multidomain particle ensembles. *Geophysical Journal International*, *155*(2),
339 479–488.
- 340 Fabian, K., & Shcherbakov, V. P. (2018). Energy barriers in three-dimensional mi-
341 cromagnetic models and the physics of thermoviscous magnetization. *Geophys-*
342 *ical Journal International*, *215*(1), 314–324. doi: 10.1093/gji/ggy285
- 343 Halgedahl, S. L. (1993). Experiments to investigate the origin of anomalously ele-
344 vated unblocking temperatures. *Journal of Geophysical Research: Solid Earth*,
345 *98*(B12), 22443–22460. doi: 10.1029/92jb02532
- 346 Heller, F., & Markert, H. (1973). The age of viscous remanent magnetization of
347 Hadrian’s Wall (Northern England). *Geophysical Journal International*, *31*(4),
348 395–406. doi: 10.1111/j.1365-246x.1973.tb06510.x
- 349 Kent, D. V. (1985). Thermoviscous remagnetization in some Appalachian lime-
350 stones. *Geophysical Research Letters*, *12*(12), 805–808. doi: 10.1029/
351 gl012i012p00805

- 352 Kronmüller, H., Schützenauer, R., & Waltz, F. (1974). Magnetic aftereffects in mag-
353 netite. *Phys. Stat. Sol. (a)*, *24*, 487-494.
- 354 Lowrie, W., & Kent, D. (1978). Characteristics of VRM in oceanic basalts. *J. Geo-*
355 *phys.*, *44*, 297-315.
- 356 Moon, T., & Merrill, R. T. (1986). A new mechanism for stable viscous remanent
357 magnetization and overprinting during long magnetic polarity intervals. *Geo-*
358 *physical Research Letters*, *13*(8), 737-740. doi: 10.1029/gl013i008p00737
- 359 Moskowitz, B. M. (1985). Magnetic viscosity, diffusion after-effect, and disaccom-
360 modation in natural and synthetic samples. *Geophysical Journal International*,
361 *82*(2), 143-161. doi: 10.1111/j.1365-246x.1985.tb05133.x
- 362 Muxworthy, A. R., Williams, J., & Heslop, D. (2015). Testing the use of viscous re-
363 manent magnetisation to date flood events. *Frontiers in Earth Science*, *3*. doi:
364 10.3389/feart.2015.00001
- 365 Muxworthy, A. R., & Williams, W. (2006). Observations of viscous magnetization
366 in multidomain magnetite. *Journal of Geophysical Research*, *111*(B1). doi: 10
367 .1029/2005jb003902
- 368 Néel, L. (1949a). Influence des fluctuations thermiques sur l'aimantation de grains
369 ferromagnétiques très fins. *J. Phys. Sér. B*, *228*, 664-666.
- 370 Néel, L. (1949b). Théorie du traînage magnétique des ferromagnétiques en grains
371 fins avec applications aux terres cuites. *Ann. Géophys.*, *5*, 99-136.
- 372 Pullaiah, G., Irving, E., Buchan, K., & Dunlop, D. (1975). Magnetization changes
373 caused by burial and uplift. *Physics of the Earth and Planetary Interiors*, *28*,
374 133-143.
- 375 Sato, T., Nakamura, N., Goto, K., Kumagai, Y., Nagahama, H., Minoura, K., ...
376 Roberts, A. P. (2019). Dating of tsunami boulders from Ishigaki Island,
377 Japan, with a modified viscous remanent magnetization approach. *Earth and*
378 *Planetary Science Letters*, *520*, 94-104. doi: 10.1016/j.epsl.2019.05.028
- 379 Sato, T., Nakamura, N., Nagahama, H., & Minoura, K. (2016). Stretched expo-
380 nential relaxation of viscous remanence and magnetic dating of erratic boul-
381 ders. *Journal of Geophysical Research: Solid Earth*, *121*(11), 7707-7715. doi:
382 10.1002/2016jb013281
- 383 Street, R., & Woolley, J. C. (1950). Time decrease of magnetic permeability in al-
384 nico. *Proceedings of the Physical Society. Section A*, *63*, 509-519.

- 385 Thellier, E. (1938). Sur l'aimantation des terres cuites et ses applications
386 géophysiques. *Ann. Inst. Phys. Globe*, *16*, 157-302.
- 387 Tivey, M., & Johnson, H. P. (1984). The characterization of viscous remanent mag-
388 netization in large and small magnetite particles. *Journal of Geophysical Re-*
389 *search*, *89*(B1), 543. doi: 10.1029/jb089ib01p00543
- 390 Williams, W., & Muxworthy, A. R. (2006). Understanding viscous magnetization
391 of multidomain magnetite. *Journal of Geophysical Research: Solid Earth*,
392 *111*(B2B02102), B02102. doi: 10.1029/2005jb003695
- 393 Yu, Y., & Tauxe, L. (2006). Acquisition of viscous remanent magnetiza-
394 tion. *Physics of the Earth and Planetary Interiors*, *159*(1-2), 32-42. doi:
395 10.1016/j.pepi.2006.05.002

Trapdoor viscous remanent magnetization

Karl Fabian¹

¹Norwegian University of Science and Technology, Department of Geoscience, S. P. Andersens veg 15a,

Trondheim, Norway

ORCID: 0000-0002-3504-3292

Key Points:

- Multidomain viscous remanent magnetization (MD VRM) is dominated by decay into trapdoor potential minima
- Previously inexplicable properties of MD VRM are explained by a quantitative trapdoor VRM theory
- Trapdoor VRM suggests an improved methodology for VRM age determination

Corresponding author: Karl Fabian, karl.fabian@ntnu.no

Abstract

Viscous remanent magnetization (VRM) in multidomain particles still exhibits many puzzling properties deviating from the current theory of VRM, based on Néel's single-domain model of magnetic particles with an almost symmetric double-well potential. In larger magnetic particles experimental evidence indicates that more complex magnetization structures preferentially change from high-energy states to low-energy states with large energy differences, such that VRM is preferentially acquired by directed magnetization changes in strongly asymmetric double-well potentials. Here a statistical model explains how this trapdoor VRM (tVRM) naturally explains the experimental observations of initial-state dependence, time-lag variation, non-linear $\log t$ dependence, and acquisition-decay asymmetry for multidomain VRM. It is discussed how tVRM can be experimentally distinguished from single-domain VRM and how the new theory can help to improve age determination by VRM analysis.

Plain Language Summary

The magnetization of rocks is an important property used to determine the history of the Earth surface and the variation of the Earth magnetic field. It is mostly stored by small magnetite particles, which still are larger than about 500 nm in diameter and are called multidomain (MD) magnetites. If a rock, after its formation, lies at the Earth surface for a long time, its magnetization slowly changes and the remanent magnetization newly acquired is called viscous remanent magnetization (VRM). This VRM is very well understood for magnetite particles below about 150 nm in diameter, but no comprehensive theory so far explains all its experimentally observed properties. Here a statistical model is developed that can explain the experimental facts and helps to understand their physical origin. The new theory allows to theoretically investigate different methods to determine the amount of time a rock was exposed to the Earth magnetic field. This leads to a better understanding of time-temperature relations for VRM, and improves the determination of relocation ages based on VRM.

1 Introduction

Viscous remanent magnetization (VRM) is generated when a rock is exposed to a magnetic field for an extended time (Thellier, 1938). Single-domain (SD) VRM is explained by Néel theory (Néel, 1949b, 1949a), but for more complex magnetization struc-

43 tures, a comprehensive theory is missing (Dunlop, 1983; Tivey & Johnson, 1984; Moskowitz,
 44 1985; Williams & Muxworthy, 2006). Dunlop (1983) finds that room-temperature (RT)
 45 VRM is unexpectedly difficult to erase by heating, and that the viscosity coefficient S
 46 increases with time, which is now termed non- $\log(t)$ behavior (Halgedahl, 1993; Williams
 47 & Muxworthy, 2006). For natural rocks, Kent (1985) confirmed that SD blocking time-
 48 temperature relaxation theory (Pullaiah et al., 1975) underestimates thermal demagne-
 49 tization temperatures in Devonian limestones. Tivey and Johnson (1984) provided ex-
 50 tensive experimental data that VRM in MD samples is sensitive to the magnetic history
 51 of the samples, and that AF demagnetization decreases, while thermal demagnetization
 52 increases the ability of MD samples to acquire VRM. Also, both MD and SD samples
 53 are sensitive to zero and weak field storage duration Δt prior to the VRM measurement
 54 (Tivey & Johnson, 1984). These effects were confirmed for various samples in subsequent
 55 experimental studies (Moskowitz, 1985; Halgedahl, 1993; Muxworthy & Williams, 2006;
 56 Williams & Muxworthy, 2006; Yu & Tauxe, 2006).

57 Moskowitz (1985) distinguishes three main physical processes for these magnetic
 58 after-effects:

- 59 1. Thermal fluctuations (Dunlop, 1973) with diffusion constants S_a for VRM acqui-
 60 sition and S_d for decay.
- 61 2. Diffusion after-effect from relaxation due to vacancy/cation diffusion across en-
 62 ergy barriers (Street & Woolley, 1950; Kronmüller et al., 1974).
- 63 3. Disaccommodation, with a relaxation equation for magnetic susceptibility.

64 Moskowitz (1985) concludes that over geologic time, thermal fluctuations dominate VRM
 65 because the other two effects have relaxation times below 10 ka.

66 Central problems for MD VRM theory are the pronounced and universal non- $\log(t)$
 67 behavior, and the dependence of VRM acquisition on initial state and on waiting time
 68 Δt . Moon and Merrill (1986) studied these effects in terms of asymmetric potentials. Mi-
 69 croscopic studies of Halgedahl (1993) and Muxworthy and Williams (2006) found episodic
 70 random domain reorganization towards more stable magnetization states. The concept
 71 of trapdoor processes in VRM acquisition first occurs in relation to the long-term VRM
 72 observations by de Groot et al. (2014). VRM overshooting first occurred in a micromag-

73 netic study by Fabian and Shcherbakov (2018) and was explained by a statistical the-
 74 ory (Fabian, 2000, 2003).

75 Improving MD VRM theory is important for Holocene age determination, indepen-
 76 dent of radionuclides (Heller & Markert, 1973; Borradaile, 1996, 2003; Muxworthy et al.,
 77 2015; Berndt & Muxworthy, 2017; Sato et al., 2019). Recent VRM models mathemat-
 78 ically modify time-temperature relations to explain observed deviations from Néel the-
 79 ory Sato et al. (2016) suggest a mathematical modification of the time-temperature re-
 80 lation, or design concrete models of MD domain wall jumps Berndt and Chang (2018).

81 Here, a simplified theory quantifies MD VRM behavior including acquisition, de-
 82 cay, reorientation, and thermoviscous relations. It predicts an exponential decay that cu-
 83 mulatively depletes excited magnetization states of increasingly higher energy barriers,
 84 and helps to infer viscous magnetization ages using a new approach that is slightly dif-
 85 ferent from Néel theory.

86 2 Viscous magnetization in a double well potential

87 Micromagnetism describes physical magnetization structures as local energy min-
 88 ima (LEM). Viscous magnetization changes through thermal activation across an energy
 89 barrier between two LEM states S_1, S_2 . In Fig. 1a, energies E_1, E_2 , and magnetic mo-
 90 ments $\mathbf{m}_1, \mathbf{m}_2$ are denoted relative to energy $E = 0$ and moment \mathbf{m}_B at the energy bar-
 91 rier maximum.

92 If the probability of being in state S_i is ρ_i , then $\rho_1 + \rho_2 = 1$, and the kinetic equa-
 93 tion for the dynamic change of ρ_1 is

$$94 \quad \tau_0 \partial_t \rho_1 = -p_{12} \rho_1 + p_{21} \rho_2 = -(p_{12} + p_{21}) \rho_1 + p_{21}. \quad (1)$$

95 Here τ_0 is the attempt period (≈ 1 ns) and p_{ij} the probability to switch from S_i into S_j
 96 during τ_0 . For weak fields \mathbf{B} , not noticeably changing the magnetization at S_1, S_2 and
 97 the saddle-point, Arrhenius equation provides

$$p_{ij} = \exp - \frac{E_i + \mathbf{m}_i \mathbf{B}}{k T}.$$

98 Setting the left hand side of (1) to zero yields equilibrium state density and magnetiza-
 99 tion

$$\bar{\rho}_1 = \frac{p_{21}}{p_{12} + p_{21}}, \quad \bar{\mathbf{m}} = \mathbf{m}_1 \bar{\rho}_1 + \mathbf{m}_2 (1 - \bar{\rho}_1).$$

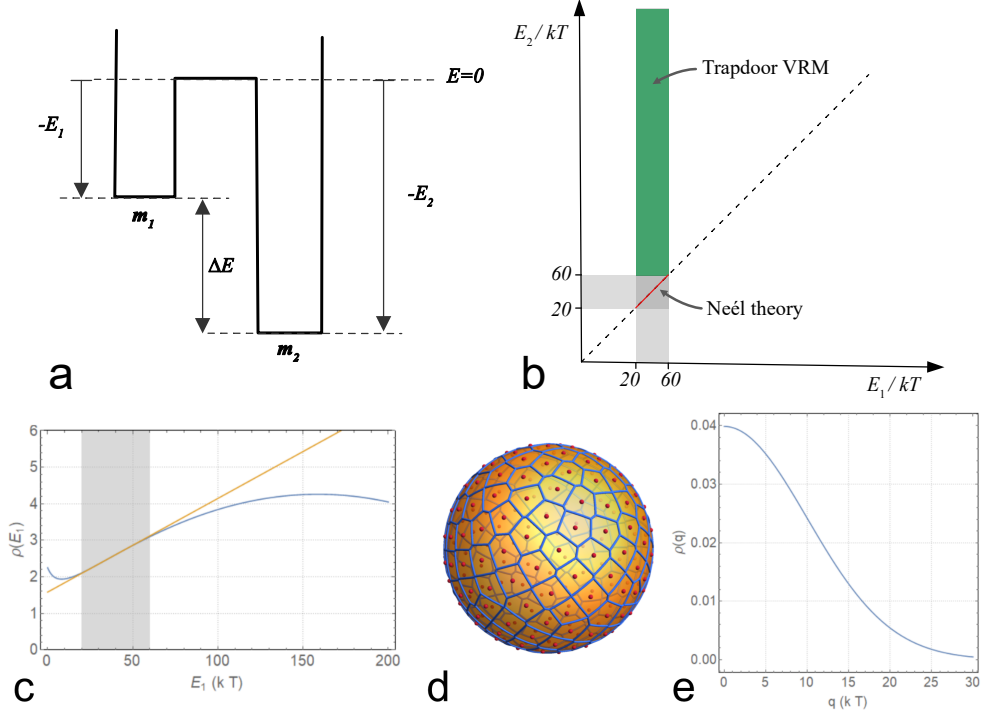


Figure 1. a) Energy barriers between two LEM states with barrier energies $E_1 \leq E_2$. In Néel-theory, the zero-field energies are equal, and the magnetic moments opposite, $E_1 = E_2$, $\mathbf{m}_1 = -\mathbf{m}_2$. For trapdoor-VRM theory it is assumed that $E_2 \gg E_1$ and no thermally activated transitions $2 \rightarrow 1$ occur. For an isotropic ensemble it then can be assumed that in the statistical average $\mathbf{m}_2 = 0$. b) Range of VRM zero-field energy barriers for Néel theory (red line) and trapdoor VRM (green). c) Approximation of a general energy barrier distribution $\psi_1(w)$ (blue) by a linear function (orange) in the small interval $[w_{\min}, w_{\max}] = [20, 60]$ (gray). d) Representation of the isotropic distribution of magnetic moment directions \mathbf{u} on the sphere by 200 nearly equi-distributed discrete directions (red) with their spherical Voronoi cells (blue). e) Gaussian distribution model of $\psi_3(q)$ for in-field energies $q > 0$ and $\sigma = 10$.

100 Solving the kinetic equation (1) for the disequilibrium density $\eta = \rho_1 - \bar{\rho}_1$, in time units
 101 of τ_0 yields

$$102 \quad \eta(t) = \eta_0 e^{-\lambda t}, \quad (2)$$

103 where

$$\lambda = p_{12} + p_{21} = \exp\left(-\frac{E_1 + \mathbf{m}_1 \mathbf{B}}{kT}\right) + \exp\left(-\frac{E_2 + \mathbf{m}_2 \mathbf{B}}{kT}\right)$$

104 is the constant of exponential decay towards $\bar{\rho}_1$. Note, that substituting λ into (2) leads
 105 to two nested exponentials which are the primary source of complications when analyz-
 106 ing VRM.

107 In Néel's theory of SD VRM (sVRM) the micromagnetic energy landscape has only
 108 two minima of equal energy $E_1 = E_2$ and opposite magnetic moments $\mathbf{m}_2 = -\mathbf{m}_1$.
 109 In contrast, trapdoor VRM (tVRM) assumes that E_1 and E_2 are very different, and math-
 110 ematically corresponds to the limit $E_2 \rightarrow \infty$ where

$$\bar{\rho}_1 \rightarrow 0, \quad \lambda \rightarrow \exp\left(-\frac{E_1 + \mathbf{m}_1 \mathbf{B}}{kT}\right).$$

111 By introducing the scaled zero-field barrier $w = E_1/(kT)$, the field energy amplitude
 112 $q = mB/(kT)$, and the angular component $\mathbf{u} \cdot \mathbf{b} = \cos\theta$ of the magnetic moment
 113 $\mathbf{m}_1 = m\mathbf{u}$ and the field $\mathbf{B} = B\mathbf{b}$, with unit vectors \mathbf{b} and \mathbf{u} , the decay constant be-
 114 comes

$$\lambda = \exp\left(-(w + q\mathbf{u} \cdot \mathbf{b})\right). \quad (3)$$

115 **3 Theory of trapdoor VRM**

116 The key observation in Néel's theory of SD TRM is that the small range 20-60 of
 117 energy barriers E/kT contains all relevant blocking times from the laboratory time scales
 118 of about 1 s to geological time-scales of 4 Ga. At RT, only these barriers contribute to
 119 VRM acquisition (Fig. 1b).

120 Only in SD or small pseudo-single domain (PSD) particles do such low barrier en-
 121 ergies systematically occur between LEMs with $E_1 \approx E_2$ (red line in Fig. 1b). In larger
 122 PSD and MD particles, it is far more likely that for the deeper LEM one has $E_2 \gg 60 kT$
 123 (green area in Fig. 1b), and with overwhelming probability, thermally activated processes
 124 only lead from the high-energy state E_1 to the low-energy state E_2 . This phenomenon
 125 has been compared to a trapdoor in de Groot et al. (2014). A specific example for a trap-
 126 door VRM process is the flower-vortex (F111-V100) transition studied and explained in

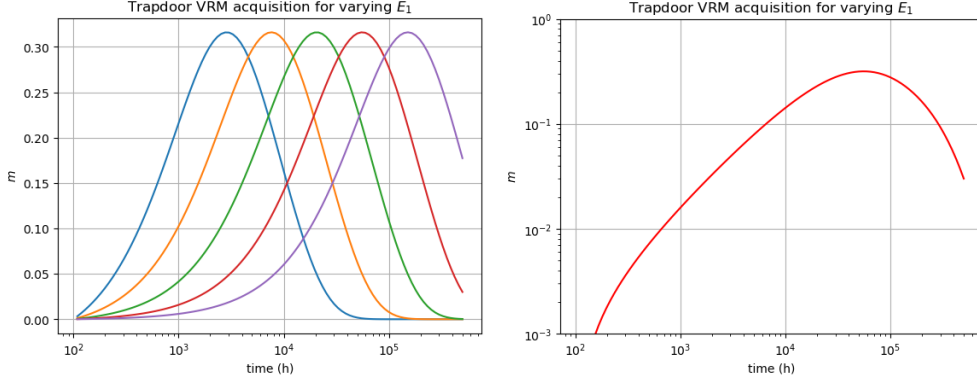


Figure 2. Left: Modeled tVRM acquisition by two oppositely magnetized states $\mathbf{u} \cdot \mathbf{b} = \pm 1$ with $q = 1 kT$ for different values of $E_1 \in [37, 38, 39, 40, 41] kT$ (blue to violet curves). Right: The log-log plot of the left red curve for $E_1 = 40 kT$ shows nearly linear increase up to about 2×10^4 h (2.3 a) due to the initial depletion of the misaligned states. Only after about 200 a also the aligned states largely are depleted.

127 Fabian and Shcherbakov (2018) based on micromagnetically calculated energy barriers
 128 of a PSD magnetite cube.

129 While sVRM results from an equilibrium within the current field, tVRM describes
 130 an irreversible depletion of high-energy LEMs, where opposite magnetizations with equal
 131 zero-field energy decay over different time scales in field. Intermediate tVRM is acquired
 132 because field-aligned states become slightly more stable, and their equally probable in-
 133 verse states decay faster. But once the field-aligned states decayed away, the final tVRM
 134 for one value of E_1 is zero. However, new intermediate tVRMs for higher energy bar-
 135 riers are synchronously acquired, such that the measured VRM over time is dynami-
 136 cally carried by different magnetic moments belonging to increasing energy barriers. Whether
 137 this on average increases the measured VRM depends on the sample-specific state-probability
 138 distribution and on the initial occupancy of the different LEMs. That an increase in VRM
 139 with time is most common is probably due to very long half-lives of misaligned moments
 140 for VRM processes with large q .

141 For example, assume two oppositely magnetized states with $E_1 = 40 kT$, $q =$
 142 $1 kT$, and $\mathbf{u} \cdot \mathbf{b} = \pm 1$. The red curve in Figure 2 displays the VRM acquired and lost
 143 by this configuration over time. In the beginning, the states acquire VRM according to
 144 a $\log t$ law because the state inverse to the external field with barrier $w - q = 39$ de-

145 cays first. After 6-7 a the field-aligned states with $w+q = 41$ also decay away and the
 146 VRM decreases until after about 100 a it has almost completely vanished. The math-
 147 ematical similarity of tVRM and radionuclide decay suggests that tVRM also may be
 148 useful for age determination.

149 **4 Modeling trapdoor VRM**

150 For quantifying tVRM it is assumed that in the parameter range of interest w , q
 151 and \mathbf{u} are statistically independent. The sample specific state-probability density then
 152 factors into

$$\psi(w, \mathbf{u}, q) = \psi_1(w) \psi_2(\mathbf{u}) \psi_3(q).$$

153 Figure 1c illustrates that the density of zero-field barriers $w = E_1/kT$ on the small in-
 154 terval $[w_{\min}, w_{\max}] = [20, 60]$, can be approximated by a linear state density

$$\psi_1(w) = \frac{1}{w_{\max} - w_{\min}} + \alpha \left(w - \frac{w_{\max} + w_{\min}}{2} \right).$$

155 For an isotropic sample, $\psi_2(\mathbf{u})$ is constant on the unit sphere. This is numerically mod-
 156 eled by a sufficiently large number of nearly equi-distributed discrete directions on the
 157 sphere, each weighted by the area of its Voronoi cell (Fig. 1d). Because the state den-
 158 sity $\psi_3(q)$ of the external-field energy q should decay away quickly for large q , it is here
 159 modeled by the positive normal distribution

$$\psi_3(q) = \frac{2}{\sqrt{2\pi} \sigma} e^{-\frac{q^2}{2\sigma^2}},$$

160 with width σ (Fig. 1e).

161 The function $\psi(w, \mathbf{u}, q)$ provides the probability for the occurrence of a LEM with
 162 parameters w , \mathbf{u} , q in the sample, but not the statistical occupancy of these states, which
 163 depends on the magnetic history of the sample. Starting from an initial state occupancy
 164 $\rho_0(w, \mathbf{u}, q)$, its evolution is described by

$$\rho(w, \mathbf{u}, q, t) = \rho_0(w, \mathbf{u}, q) \psi(w, \mathbf{u}, q) \exp\left(-t e^{-(w+q(\mathbf{u}\cdot\mathbf{b}))}\right). \quad (4)$$

165 The numerical models below assume an initially constant state occupancy ρ_0 on the rel-
 166 evant tVRM parameter interval, which approximately represents a thermally demagne-
 167 tized or a weak field TRM state, assuming that the TRM reflects only a small deviation
 168 from the equilibrium absolute zero state. AF demagnetized or ARM states may have dif-
 169 ferent initial state occupancies, where low energy barriers w and larger q states are less

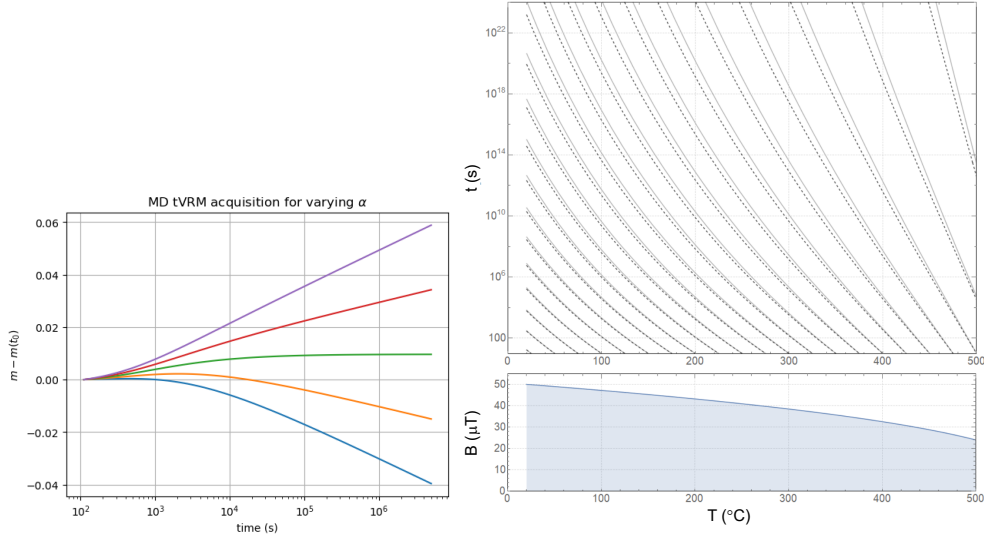


Figure 3. Left: Modeled tVRM acquisition for different values of α in the state-probability $\psi_1(w)$. The shown model uses the parameters $\sigma = 5$, $w \in [20, 80]$ and $\alpha = [-1, -0.5, 0, 0.5, 1]/(w_{max} - w_{min})^2$ for the plots from blue to violet. The model run starts after an initial 500 s VRM acquisition. Note that a decreasing state-probability with increasing w (blue, orange) can lead to decreasing VRM in a positive field, due to the fact that depletion of the field mis-aligned low- w states is not dynamically balanced by larger VRM acquisition of high- w barriers. Right top: Time-temperature diagram for tVRM decay times in MD magnetite calculated using equation (6) for two different critical exponents γ of $M_s(T)$: $\gamma = 0.38$ (solid gray), $\gamma = 0.36$ (dashed). Right bottom: Required change of applied field as a function of temperature to retain correct tVRM scaling for initial field $B_0 = 50 \mu\text{T}$ at RT.

170 populated than larger w and lower q states. In very old rocks, the 'trapdoor'-components
 171 of VRM are already largely activated and trapped in their low-energy minima, such that
 172 ρ_0 will be extremely reduced for smaller w .

173 **5 Recovering the tVRM activation history**

174 Because tVRM is a combination of many simple decay processes, to recover the VRM
 175 history of a rock, it appears promising to measure which energy levels of LEMs have al-
 176 ready been depleted during the time of the rock emplacement. The simplest procedure
 177 to measure this would be to again acquire VRM in the same external field for an extended
 178 period of time and then identify at what point an increase in VRM acquisition is detected.
 179 At this time, new LEM barriers that have not been depleted previously are activated.

180 Curves like those in Fig. 4 (top right) can then be used to calibrate the experimental data,
 181 and infer a viscous-remanence age from the rock.

182 Unfortunately, VRM of interesting processes was acquired on historical and geo-
 183 logical time scales, such that this direct approach is not practical and needs to be replaced
 184 by an alternative way to activate higher energy barriers. The classical procedure in Néel
 185 theory is to increase the measurement temperature and use time-temperature relations
 186 (Pullaiah et al., 1975; Heller & Markert, 1973) to convert between these quantities.

187 For tVRM acquired by MD magnetite well below the Curie temperature $T_C \approx 580^\circ\text{C}$
 188 the zero-field micromagnetic energy is dominated by the demagnetizing energy which scales
 189 with $K_d(T) = \frac{1}{2} \mu_0 M_s(T)^2$, such that

$$\frac{E_1(T)}{K_d(T)} = w \frac{kT}{K_d(T)}$$

190 is almost independent of T . Using the saturation magnetization $M_{s,0}$ at 0 K, and the
 191 critical exponent $\gamma \approx 0.37$ one has

$$M_s(T) = M_{s,0} (1 - T/T_C)^\gamma,$$

192 and with

$$\beta(T) = \frac{kT}{K_d(T)} \frac{K_d(T_0)}{kT_0} = \frac{T}{T_0} \left(\frac{T_C - T_0}{T_C - T} \right)^{2\gamma},$$

193 one can write $w(T) \approx w\beta(T)$. In experiments the same scaling behavior for $q = mB$
 194 is achieved by decreasing the applied field strength according to

$$195 \quad B(T) = B(T_0) \frac{M_s(T)}{M_s(T_0)}. \quad (5)$$

196 The temperature dependence of the decay constant in (3) is then

$$\lambda(T) = \lambda^{\beta(T)}.$$

197 If at temperature T , the laboratory decay time $t_L = 1/\lambda(T)$ activates the same
 198 energy barriers as a RT decay time of $t = 1/\lambda(T_0)$ one gets

$$\frac{\log t/\tau_0}{\log t_L/\tau_0} \approx \frac{1}{\beta(T)}.$$

199 For $t_L = 10$ s one has $\log t_L/\tau_0 = 23$ with the time-temperature relation

$$\log t/\tau_0 \approx 23 \frac{T M_s^2(T_0)}{T_0 M_s^2(T)}. \quad (6)$$

200 This agrees with the time-temperature relation derived from Néel theory for pure shape
 201 anisotropy (Pullaiah et al., 1975), because also in this case only demagnetizing energies
 202 are considered. Yet, equation (6) applies to different magnetization processes where the
 203 laboratory field is aligned with the natural VRM overprinting field and changes accord-
 204 ing to the scaling (5). The cumulative depletion of high-energy LEMs generates a sub-
 205 stantially different magnetization behavior than the predictions based on Néel theory,
 206 although also in the sVRM case for magnetite, VRM at elevated temperatures should
 207 be acquired in the correctly scaled field $B(T)$.

208 Fig. 3(right) demonstrates that this relation predicts a sensitive dependence of tVRM
 209 acquisition on temperature and heating rate. Using thermal tVRM acquisition as a dat-
 210 ing tool therefore requires very careful experiments allowing for accurate control of the
 211 measurement conditions in terms of temperature, measurement time, and thermal equi-
 212 libration.

213 In the supplementary material the Python code for a numerical model is provided
 214 that allows to simulate arbitrary time-temperature and field histories for magnetite MD
 215 ensembles based on the assumption of initially nearly constant probability density.

216 If the magnetization of a rock was displaced from an initial orientation \mathbf{m}_A to a
 217 new orientation \mathbf{m}_B it starts to realign its VRM with the current field H .

218 6 Discussion

219 The tVRM model describes a depletion of LEM states with elevated energy by means
 220 of a decay equation, and appears simpler than Néel's sVRM theory. What complicates
 221 the tVRM model, is the statistical decoupling of magnetic moment vectors and energy
 222 barriers. The corresponding evolution of $\rho(w, \mathbf{u}, q, t)$ naturally explains the experimen-
 223 tally observed deviations of MD VRM from Néel theory. The modeling of tVRM is com-
 224 plex, because the integration over the decay equations for all energy barriers and mag-
 225 netic moments cannot be done analytically and requires numerical treatment. The most
 226 notable property of tVRM is that it statistically approaches zero as depicted in Fig. 2,
 227 whilst sVRM attains a non-zero equilibrium. The visible tVRM is carried by changing
 228 magnetic moments from successively increasing energy barriers. Accordingly, the VRM
 229 magnetization curves depend on the distribution and initial occupation of these energy
 230 barriers. In Fig. 3(left) the dependence of the slope of the tVRM acquisition curves on

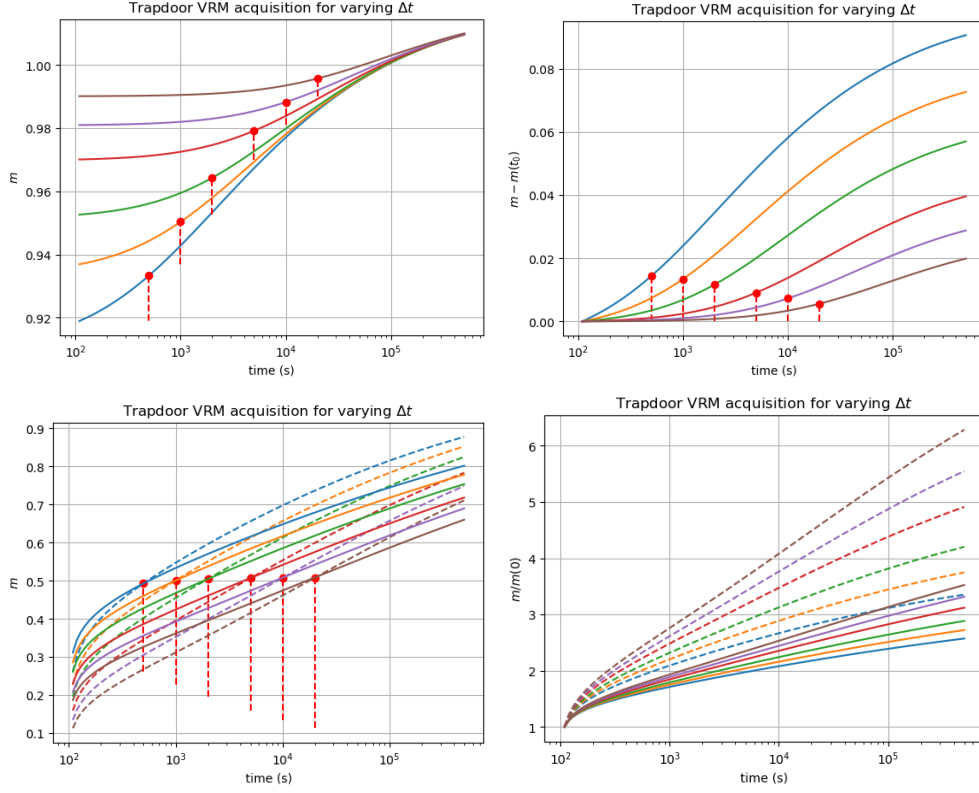


Figure 4. Top left: Modeled tVRM acquisition in an MD sample with initial density defined by $\alpha = 0$, $\sigma = 10$ and VRM acquisition in x-direction for $\Delta t = 0.5, 1, 2, 5, 10, 20 \times 10^3$ s (sequence blue to brown). The plot shows the results of a repeated VRM acquisition in x-direction after this history. Note the marked non- $\log(t)$ behavior and the systematic dependence on the previous Δt marked by red dots. Top right: The same data after subtracting the initial magnetization to simplify comparison to experiments. Bottom Left: Same as top left, but with initial density after VRM in zero field (dashed lines) or in perpendicular y -direction (solid lines) for $\Delta t = 0.5, 1, 2, 5, 10, 20 \times 10^3$ s (sequence blue to brown). Bottom right: The same data as on the left after subtracting the initial magnetization.

231 the slope α of the zero-field energy distribution $\psi_1(w)$ is plotted. The results demonstrate
 232 that tVRM acquired in a positive field may even decrease with time. To what extent de-
 233 tails of the distributions ψ_1 and ψ_3 systematically depend on grain size, shape or other
 234 average quantities of the magnetic particle ensemble is unclear and requires further study,
 235 preferably by micromagnetic models (Conbhuí et al., 2018; Fabian & Shcherbakov, 2018).

236 A significant deviation from Néel theory is that MD VRM acquisition strongly de-
 237 pends on initial state. sVRM usually starts from a near equilibrium of two equal zero-
 238 field energy states, and evolves towards an only slightly different equilibrium. In con-
 239 trast, tVRM is a pure depletion process modified by the external field. Figure 4 displays
 240 model runs which demonstrate that tVRM acquisition depends strongly on the initial
 241 population of the high-energy LEMs. The top row shows tVRM acquisition curves af-
 242 ter a previous tVRM acquisition in the same direction, that partly depleted the low- w
 243 states with field-aligned magnetic moments. tVRM during a second acquisition in the
 244 same direction depends on the degree of the first depletion and leads to s-shaped acqui-
 245 sition curves, resembling various experimental results, for example in figures 4,6,7 of (Moskowitz,
 246 1985), figure 2 in (Bikova & Igoshin, 1985), and figures 1,8 in (Lowrie & Kent, 1978).

247 High activation energy during AF demagnetization of MD samples leads to a lower
 248 occupation probability of low- w LEMs than thermal demagnetization. This explains why
 249 AF or ARM states in MD samples acquire less VRM than thermally demagnetized or
 250 TRM states.

251 The tVRM model calculations can show both, marked non- $\log t$ behavior and straight
 252 $\log t$ behavior, at least over extended time intervals. Non- $\log t$ behavior typically results
 253 from partly depleted initial states, where over long time-scales larger energy barriers are
 254 activated, that block LEMs with higher occupation probability. Another source of non-
 255 $\log t$ behavior can be strongly varying energy barrier distributions in the active region.
 256 For tVRM the physical origin of the magnetic energy barrier is irrelevant for the statis-
 257 tical behavior of the sample, such that also diffusion after-effects from vacancy or cation
 258 diffusion (Street & Woolley, 1950; Kronmüller et al., 1974) and disaccommodation pro-
 259 cesses (Moskowitz, 1985) are described by the tVRM model. On some time scales these
 260 effects may substantially increase the energy barrier density.

261 The waiting time Δt effect in principle occurs even for the simple $\log t$ -law

$$M(t) - M_0 = S \log t, \text{ for } t > t_0,$$

262 because it predicts a VRM

$$M_{\Delta t}(t) = M(t + \Delta t) - M(\Delta t) \approx M(t) - S \log(\Delta t),$$

263 that shows a 'hardening effect' (Dunlop, 1983) due to the asymptotic downward shift $S \log \Delta t$.

264 The tVRM model predicts a a strong Δt effect due to the irreversible depletion of LEMs
 265 in contrast to the reversible equilibrium shift in the sVRM model. This is leads to a sys-
 266 tematic variation in Fig. 4 which contains plots of modeled tVRM acquisitions after dif-
 267 ferent previous acquisition periods Δt .

268 **6.1 Combinations of sVRM and tVRM**

269 In samples with different magnetic grain size populations, both types, sVRM and
 270 tVRM, may be present in various combinations. Especially for age determination, it is
 271 of interest to separate these two components into

$$VRM = sVRM + tVRM.$$

272 To design methods to identify the more reversible behavior of sVRM is the aim of fu-
 273 ture experimental studies. The region in Fig. 1b off the red diagonal, where both asym-
 274 metric barriers are below $60 kT$ may require separate treatment in certain narrow PSD
 275 particle ensembles. This requires the more comprehensive but also more complex Markov
 276 chain methods (Fabian & Shcherbakov, 2018). The simpler theory of tVRM focuses on
 277 MD particle ensembles, and on ensembles with large grain size variation.

278 The observation that isothermal VRM is overly difficult to erase by heating (Dunlop,
 279 1983; Kent, 1985) finds a natural explanation in tVRM, where a magnetic moment is al-
 280 most impossible to move back from a trapped state. To erase such a tVRM with bar-
 281 rier $w-q$ it is necessary that the field-aligned magnetizations with their larger in-field
 282 barrier $w+q$ or zero-field barrier w also decay into their trapped states, which requires
 283 higher temperatures than expected for a $w - q$ barrier.

284 Because tVRM results from a dynamic decay that depletes the occupation prob-
 285 abilities for successively larger energy barriers w , those low- w LEMs that have been de-
 286 pleted cannot be easily occupied again. It is therefore possible to experimentally deter-
 287 mine the degree of depletion, and from that infer the time it took to reach this state of
 288 depletion. To do this one has to find a measurable difference between depleted and oc-
 289 cupated LEMs, which naively can be done by simply repeating the VRM acquisition in

290 the same external field, and wait until an accelerated tVRM acquisition is observed. Of
 291 course, waiting times of thousands of years are unpractical, and thus the time-temperature
 292 relation (6) can be used to replace waiting time through measurements at elevated tem-
 293 peratures. To keep the correct scaling, the applied field strength in these measurements
 294 must be scaled down, according to (5). Calibration curves for such dating methods, could
 295 be developed based on the here presented programs and additional rock magnetic mea-
 296 surements that constrain the LEM state-distribution function ψ .

297 If tVRM prevails in a rock sample, its VRM acquisition depends strongly on the
 298 initial occupation and state-densities ρ_0, ψ , and there exists little reliable data to real-
 299 istically constrain these functions. Thus, the tVRM concept provides a new incentive and
 300 guideline to design targeted experimental and micromagnetic studies to determine re-
 301 alistic density distributions ψ_1 and ψ_3 . This will enable a better understanding of VRM
 302 processes, improve existing and help to develop new methods of age determination, ei-
 303 ther directly based on tVRM, or by better isolating the contribution of sVRM.

304 7 Open Research

305 The Python code used to model the VRM processes is available in the supporting
 306 information. If requested, the code will eventually be deposited at the NTNU repository
 307 (dataverse.no) by the time the article is accepted.

308 Acknowledgments

309 References

- 310 Berndt, T., & Chang, L. (2018). Theory of stable multi-domain thermoviscous rema-
 311 nence based on repeated domain-wall jumps. *Journal of Geophysical Research:*
 312 *Solid Earth*. doi: 10.1029/2018jb016816
- 313 Berndt, T., & Muxworthy, A. R. (2017). Dating Icelandic glacial floods using a new
 314 viscous remanent magnetization protocol. *Geology*, *45*(4), 339–342. doi: 10
 315 .1130/g38600.1
- 316 Bikova, E., & Igoshin, L. (1985). On the interrelation between magnetic viscos-
 317 ity and the compositions of magnetites in the alkali-ultrabasic rocks the Kola
 318 peninsula. *Izvestiya. Earth Phys.*, *21*, 794-800.

- 319 Borradaile, G. J. (1996). An 1800-year archeological experiment in remagnetization.
320 *Geophysical Research Letters*, *23*(13), 1585–1588. doi: 10.1029/96gl01575
- 321 Borradaile, G. J. (2003). Viscous magnetization, archaeology and Bayesian statis-
322 tics of small samples from Israel and England. *Geophysical Research Letters*,
323 *30*(10), 4. doi: 10.1029/2003gl016977
- 324 Conbhuí, P. Ó., Williams, W., Fabian, K., Ridley, P., Nagy, L., & Muxworthy,
325 A. R. (2018). MERRILL: Micromagnetic earth related robust interpreted
326 language laboratory. *Geochemistry, Geophysics, Geosystems*, *19*. doi:
327 10.1002/2017gc007279
- 328 de Groot, L. V., Fabian, K., Bakelaar, I. A., & Dekkers, M. J. (2014). Magnetic
329 force microscopy reveals meta-stable magnetic domain states that prevent
330 reliable absolute palaeointensity experiments. *Nature Communications*, *5*.
- 331 Dunlop, D. J. (1973). Theory of the magnetic viscosity of lunar and terrestrial rocks.
332 *Reviews of Geophysics*, *11*(4), 855. doi: 10.1029/rg011i004p00855
- 333 Dunlop, D. J. (1983). Viscous magnetization of 0.04–100 μm magnetites. *Geophys.*
334 *J. R. astr. Soc.*, *74*(4), 667–687.
- 335 Fabian, K. (2000). Acquisition of thermoremanent magnetization in weak magnetic
336 fields. *Geophysical Journal International*, *142*(2), 478–486.
- 337 Fabian, K. (2003). Statistical theory of weak field thermoremanent magnetization
338 in multidomain particle ensembles. *Geophysical Journal International*, *155*(2),
339 479–488.
- 340 Fabian, K., & Shcherbakov, V. P. (2018). Energy barriers in three-dimensional mi-
341 cromagnetic models and the physics of thermoviscous magnetization. *Geophys-*
342 *ical Journal International*, *215*(1), 314–324. doi: 10.1093/gji/ggy285
- 343 Halgedahl, S. L. (1993). Experiments to investigate the origin of anomalously ele-
344 vated unblocking temperatures. *Journal of Geophysical Research: Solid Earth*,
345 *98*(B12), 22443–22460. doi: 10.1029/92jb02532
- 346 Heller, F., & Markert, H. (1973). The age of viscous remanent magnetization of
347 Hadrian’s Wall (Northern England). *Geophysical Journal International*, *31*(4),
348 395–406. doi: 10.1111/j.1365-246x.1973.tb06510.x
- 349 Kent, D. V. (1985). Thermoviscous remagnetization in some Appalachian lime-
350 stones. *Geophysical Research Letters*, *12*(12), 805–808. doi: 10.1029/
351 gl012i012p00805

- 352 Kronmüller, H., Schützenauer, R., & Waltz, F. (1974). Magnetic aftereffects in mag-
353 netite. *Phys. Stat. Sol. (a)*, *24*, 487-494.
- 354 Lowrie, W., & Kent, D. (1978). Characteristics of VRM in oceanic basalts. *J. Geo-*
355 *phys.*, *44*, 297-315.
- 356 Moon, T., & Merrill, R. T. (1986). A new mechanism for stable viscous remanent
357 magnetization and overprinting during long magnetic polarity intervals. *Geo-*
358 *physical Research Letters*, *13*(8), 737-740. doi: 10.1029/gl013i008p00737
- 359 Moskowitz, B. M. (1985). Magnetic viscosity, diffusion after-effect, and disaccom-
360 modation in natural and synthetic samples. *Geophysical Journal International*,
361 *82*(2), 143-161. doi: 10.1111/j.1365-246x.1985.tb05133.x
- 362 Muxworthy, A. R., Williams, J., & Heslop, D. (2015). Testing the use of viscous re-
363 manent magnetisation to date flood events. *Frontiers in Earth Science*, *3*. doi:
364 10.3389/feart.2015.00001
- 365 Muxworthy, A. R., & Williams, W. (2006). Observations of viscous magnetization
366 in multidomain magnetite. *Journal of Geophysical Research*, *111*(B1). doi: 10
367 .1029/2005jb003902
- 368 Néel, L. (1949a). Influence des fluctuations thermiques sur l'aimantation de grains
369 ferromagnétiques très fins. *J. Phys. Sér. B*, *228*, 664-666.
- 370 Néel, L. (1949b). Théorie du traînage magnétique des ferromagnétiques en grains
371 fins avec applications aux terres cuites. *Ann. Géophys.*, *5*, 99-136.
- 372 Pullaiah, G., Irving, E., Buchan, K., & Dunlop, D. (1975). Magnetization changes
373 caused by burial and uplift. *Physics of the Earth and Planetary Interiors*, *28*,
374 133-143.
- 375 Sato, T., Nakamura, N., Goto, K., Kumagai, Y., Nagahama, H., Minoura, K., ...
376 Roberts, A. P. (2019). Dating of tsunami boulders from Ishigaki Island,
377 Japan, with a modified viscous remanent magnetization approach. *Earth and*
378 *Planetary Science Letters*, *520*, 94-104. doi: 10.1016/j.epsl.2019.05.028
- 379 Sato, T., Nakamura, N., Nagahama, H., & Minoura, K. (2016). Stretched expo-
380 nential relaxation of viscous remanence and magnetic dating of erratic boul-
381 ders. *Journal of Geophysical Research: Solid Earth*, *121*(11), 7707-7715. doi:
382 10.1002/2016jb013281
- 383 Street, R., & Woolley, J. C. (1950). Time decrease of magnetic permeability in al-
384 nico. *Proceedings of the Physical Society. Section A*, *63*, 509-519.

- 385 Thellier, E. (1938). Sur l'aimantation des terres cuites et ses applications
386 géophysiques. *Ann. Inst. Phys. Globe*, 16, 157-302.
- 387 Tivey, M., & Johnson, H. P. (1984). The characterization of viscous remanent mag-
388 netization in large and small magnetite particles. *Journal of Geophysical Re-*
389 *search*, 89(B1), 543. doi: 10.1029/jb089ib01p00543
- 390 Williams, W., & Muxworthy, A. R. (2006). Understanding viscous magnetization
391 of multidomain magnetite. *Journal of Geophysical Research: Solid Earth*,
392 111(B2B02102), B02102. doi: 10.1029/2005jb003695
- 393 Yu, Y., & Tauxe, L. (2006). Acquisition of viscous remanent magnetiza-
394 tion. *Physics of the Earth and Planetary Interiors*, 159(1-2), 32-42. doi:
395 10.1016/j.pepi.2006.05.002

Supplement to
'Trapdoor viscous remanent magnetization'

Karl Fabian
NTNU, S. P. Andersens veg 15a, Trondheim, Norway
karl.fabian@ntnu.no

October 2023

1 Description of Python routines for trapdoor VRM

The following Python routines are used to model trapdoor VRM processes. The corresponding Jupyter notebooks are provided.

1.1 Nearly uniform distribution of points on the sphere

The first function is generating a numpy array of unit vectors in three dimensions, that nearly uniformly covers the unit sphere and contains for each vector also the antipodal vector.

```
1 import numpy as np
2 import matplotlib.pyplot as plt
3 from scipy.spatial import SphericalVoronoi
4 import math
5 from numba import njit
6
7 def fibonacci_symsphere(samples=100): # Points on a sphere
8     # distributed by golden section spiral, but with exact antipodes
9
10    points = []
11    phi = math.pi * (math.sqrt(5.) - 1.) # golden angle in radians
12
13    for i in range(samples):
14        z = 1 - (i / float(samples - 1)) # z goes from 1 to 0
15        radius = math.sqrt(1 - z * z) # radius at z
16
17        theta = phi * i # golden angle increment
18
19        x = math.cos(theta) * radius
20        y = math.sin(theta) * radius
21
22        points.append((x, y, z)) # add point
23        points.append((-x, -y, -z)) # add antipode
24
25    return np.array(points) # returns 2 * samples points !!
```

1.2 Fast calculation of trapdoor VRM

To use the numba in-place compiler '@njit' for accelerating the nested summing involved in tVRM calculation, a fast function is defined that lies outside the later defined class 'Trap_VRM_Density'. This function performs the main task in tVRM modeling by updating the occupation ρ for each parameter combination of barrier w (E1), magnetic moment energy q (MH), and magnetic moment direction \mathbf{u} (dirs[k] weighted by dir_weights[k]). The updating is done by performing a time step t of the exponential decay using the individually calculated appropriate decay constant p_{12} . The loop also calculates the average magnetic moment after the time step by adding all moments $q\mathbf{u}$ with their correct weight and occupation density.

```

1 @njit
2 def _fast_Trap(b,m,d,fd,t,E1,MH,dirs,rho,dir_weights):
3     avmag=np.zeros(3)
4     for i in range(b):
5         for j in range(m):
6             for k in range(d):
7                 p12=np.exp(-(E1[i]+MH[j]*np.dot(fd,dirs[k]))) #
8                 decay constant for specific barrier
9                 rho[i,j,k]*=np.exp(-p12*t) # updating decay of
10                state density during time t
11                avmag+=dirs[k]*MH[j]*rho[i,j,k]*dir_weights[k] #
12                contribution to total magnetization
13            return avmag

```

1.3 Trapdoor VRM density class

The main functions to define and calculate tVRM models are encapsulated in the 'Trap_VRM_Density' class. It has three parameters containing the list of energy barriers w , the list of q values and the list of magnetic moment directions \mathbf{u} . With initialization the lengths of these lists are calculated and also the weights of the individual directions through the area of their spherical Voronoi cell. Initially a constant density is assigned to all states, but this can be changed to the density described in the main article by calling the function 'set_density' which requires α and σ as parameters. The evolution of the state occupation ρ is performed through the function 'density_evolve' that also uses the helper function 'time_rescale' to convert the human readable time scales m,h,d,a,ka,Ma,Ga into multiples of τ_0 . The computationally challenging part of 'density_evolve' is performed by calling the previously described '_fast_Trap' function.

```

1 class Trap_VRM_Density:
2     def __init__(self, bar, mag, directions):
3         self.b=np.shape(bar)[0] # Length of energy barrier list
4         self.m=np.shape(mag)[0] # Length of magnetic field energy
5         list (for given h)
6         self.d=np.shape(directions)[0] # Number of directions on
7         the sphere
8
9         self.w_min=bar[0]
10        self.w_max=bar[-1]
11
12        self.t0= 1e-9 # tau0 in unit seconds
13
14        self.E1 = bar # Energy barrier list in units k T
15        self.MH = mag # Magnetic field energy list (for given h)
16        in units k T
17        self.dirs =directions # Direction unit vectors on the
18        sphere
19        try:
20            sv = SphericalVoronoi(directions, 1, np.array([0, 0,
21            0])) # Voronoi tessellation with these centers
22            self.dir_weights=sv.calculate_areas()/4/np.pi #
23            Weights of all Voronoi cells
24        except:

```

```

20         self.dir_weights=np.array([1 for dd in self.dirs])/np.
        shape(self.dirs)[0]
21
22         self.constant_density()
23
24
25     def constant_density(self):
26         self.rho = np.ones((self.b,self.m,self.d)) # all
        combinations are assumed to have the same initial probability
27         self.history=[[ 'constant density']] # clear history
28
29     def set_density(self,alpha,sigma ):
30         self.rho = np.ones((self.b,self.m,self.d)) # all
        combinations are assumed to have the same initial probability
31         i=0; j=0; k=0
32         for i in range(self.b):
33             rw= 1/(self.w_max-self.w_min)+ alpha * (self.E1[i
        ]-0.5*(self.w_max+self.w_min))/(self.w_max-self.w_min)/(self.
        w_max-self.w_min)
34             rw=2*rw/(sigma)/np.sqrt(2*np.pi) # normalization
        parameter depends on i only
35             for j in range(self.m):
36                 rq=rw*np.exp(-0.5*self.MH[j]*self.MH[j]/sigma/sigma
        )
37                 for k in range(self.d):
38                     self.rho[i,j,k]= rq
39
40
41         self.history=[[ 'density reset',alpha,sigma]] # clear
        history
42
43     def time_rescale(self,t,t_unit):
44         if t_unit=='a':
45             t*=60*60*24*365.25
46         if t_unit=='m':
47             t*=60
48         if t_unit=='h':
49             t*=60*60
50         if t_unit=='d':
51             t*=60*60*24
52         if t_unit=='ka':
53             t*=60*60*24*365.25*1000
54         if t_unit=='Ma':
55             t*=60*60*24*365.25*1.e6
56         if t_unit=='Ga':
57             t*=60*60*24*365.25*1.e9
58         t/=self.t0 # time now in units of tau0
59         return t
60
61     def density_evolve(self,tval,t_unit,field_dir):
62         t= self.time_rescale(tval,t_unit) # time in units of tau_0
63         fd=1.0*np.array(field_dir) # non-normalized field
        direction e.g. [1,1,1]
64         norm=np.linalg.norm(fd)
65         if (norm>0.0001): # allows for zero field in case of
        viscous decay
66             fd/=norm # unit vector in field direction

```

```
67
68     avmag=_fast_Trap(self.b,self.m,self.d,fd,t,self.E1,self.MH,
69     self.dirs,self.rho,self.dir_weights)
70     self.history.append([tval,t_unit,field_dir,t,avmag])
    return avmag
```

2 Additional figures

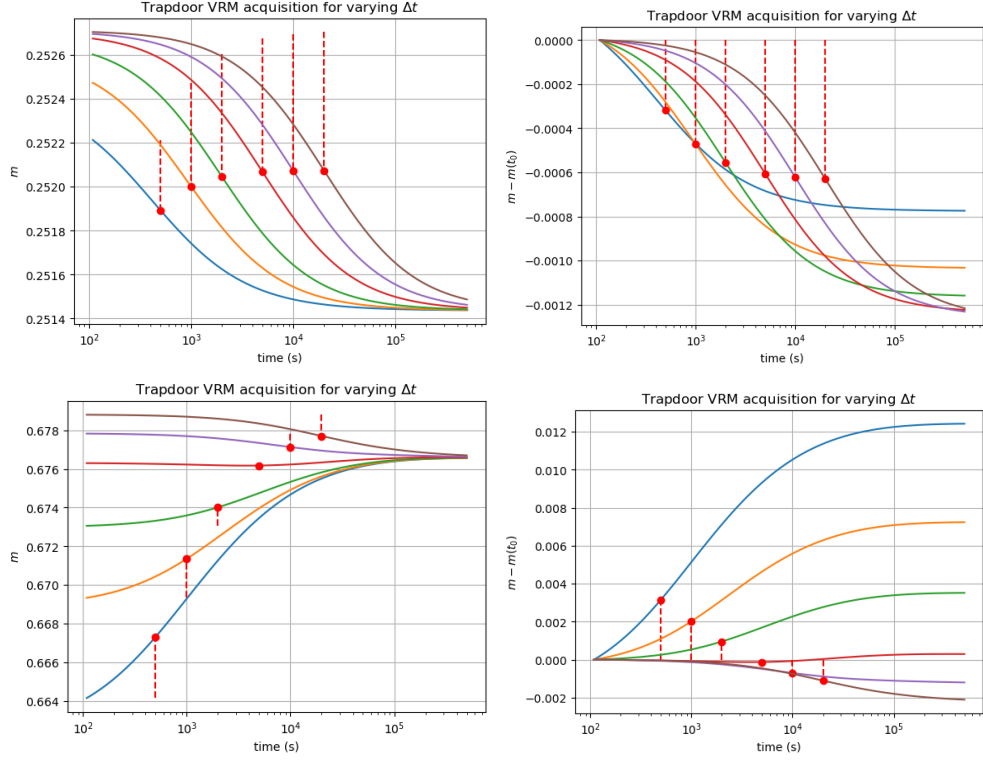


Figure 1: Top left: Modeled tVRM acquisition in an MD sample with initial density defined by $\alpha = 0$, $\sigma = 3$ and VRM acquisition in x-direction for $\Delta t = 0.5, 1, 2, 5, 10, 20 \times 10^3$ s (sequence blue to brown). The plot shows the results of a repeated VRM acquisition in x-direction after this history. Note the marked non- $\log(t)$ behavior and the systematic dependence on the previous Δt marked by red dots. Top right: The same data after subtracting the initial magnetization to simplify comparison to experiments. Bottom Left: Same as top left, but with initial density defined by $\alpha = 0$, $\sigma = 3$ for $\Delta t = 0.5, 1, 2, 5, 10, 20 \times 10^3$ s (sequence blue to brown). Bottom right: The same data as on the left after subtracting the initial magnetization.